Geomechanics and Engineering, *Vol. 16, No. 4 (2018) 341-353*
DOI: https://doi.org/10.12989/gae.2018.16.4.341

Train induced dynamic response of a pedestrian tunnel under a four-track surface railway for different soil water contents

Ahmed Abdelraheem Farghaly[1a] and Denise-Penelope N. Kontoni[*2]

[1]*Department of Civil and Architectural Constructions, Faculty of Industrial Education, Sohag University, Sohag 82524, Egypt*
[2]*Department of Civil Engineering, Technological Educational Institute of Western Greece, 1 M. Alexandrou Str., Koukouli, GR-26334 Patras, Greece*

(Received May 9, 2018, Revised June 14, 2018, Accepted June 20, 2018)

Abstract. A reinforced concrete pedestrian tunnel is constructed under a four-track surface railway. Heavy rainfall and soil exposure to drying lead to soil with different water content throughout the year. A railway is an open utility that is subject to rainfall without control on the quantity of the water on it and when there is a tunnel under a railway, the water content of the soil around the tunnel is very influential. This research shows the effects of change of water content in the soil around a pedestrian tunnel under a four-track surface railway. The pedestrian tunnel and the soil block around the tunnel are modeled in 3D by the FEM and are studied under the vibrations induced by the moving trains on the four-track surface railway for different soil water contents and the effects of the soil water content on the dynamic behavior of the tunnel and the surrounding soil are demonstrated.

Keywords: pedestrian tunnel; four-track surface railway; moving trains induced vibrations; soil water content; dynamic analysis; FEM

1. Introduction

A reinforced concrete (RC) pedestrian tunnel is constructed in Sohag, Egypt, under the four-track surface railway. The problem of the soil in many structures is the lack of control of changing the values of water content in the soil for several reasons, whether the level of groundwater or because of rainfall on the soil. The surface railway is an open utility which is subjected to rainfall without control on the quantity of the water on it and when there is a tunnel under the railway, the effect of the soil around the tunnel is very influential. The rainfall, even so, it is rare in Upper Egypt, it comes as a torrent by a very big quantity so the soil under the railway and around the tunnel will be saturated by the water and after that will suffer from the drying process which will change the water contents with changing the dynamic properties of the soil especially with vibrations induced by moving trains passing over the tunnel region.

Zhao *et al.* (2017) checked the performance of reinforced concrete linings of shield tunnels and proved that the tunnel lining is more vulnerable under lateral unloading due to excavation on both tunnel sides than underground overloading on the top of the tunnel.

Aksoy *et al.* (2016) applied the "Non-Deformable Support System" analysis method to the tunnel-34 of Ankara-Istanbul railway and showed that the results coincide with the in-situ measurements.

Han *et al.* (2016) studied a method of design for a very long submerged floating tunnel subjected to earthquake by a model order reduction technique and proved that this method can efficiently be applied with a good accuracy in designing such structures.

Zhou *et al.* (2016) studied the exit portal of an express railway tunnel with a bridge-tunnel combination; the stability of the slope on which the railway portal was built was analyzed using 3D numerical simulation and the results obtained can be used to guide the structural design and construction of such structures.

Cui *et al.* (2017) studied the deformation of concrete for shotcrete use in hot-humid and hot-dry tunnel environments.

Jafarnia and Varzaghani (2016) studied the effect of near-field earthquake on the monuments adjacent to underground tunnels using a hybrid Finite Element Analysis-Neural Network technique.

Öztürk *et al.* (2016) studied the optimum cost design of cut and cover reinforced concrete shallow tunnels using artificial bee colony and genetic algorithms.

Ding *et al.* (2013) investigated the segment joint in shield TBM tunnel lining construction and proposed a mechanical model which was verified by full-scale tests.

Zheng *et al.* (2017) studied the effect of excavations on adjacent tunnels and also they provided design charts and tables; the proposed FEM techniques indicated that the deformation mode of the retaining structure has a significant influence on the deformation of certain tunnels.

Yang and Li (2017) applied the reliability analysis on a shallow tunnel with surface settlement and it is found that

*Corresponding author, Associate Professor
E-mail: kontoni@teiwest.gr
[a]Associate Professor
E-mail: farghaly@techedu.sohag.edu.eg

ISSN: 2005-307X (Print), 2092-6219 (Online)

the unit weight significantly affects the reliability index; the reliability index for tunnel support pressure with different situations was obtained and the required tunnel support pressure can be calculated.

Ding *et al.* (2017) investigated the ground surface settlement due to tunnel-excavation and succeeded in an effective prediction of the surface settlement caused by tunnel construction around an adjacent building.

Yuan *et al.* (2016) presented a modified grey clustering method to evaluate the risk of water inrush in karst tunnels and found that the proposed risk assessment methodology provides a powerful tool for engineers.

Khezri *et al.* (2016) investigated the 3D stability of a shallow circular tunnel in a layered soil and found that the ratio of the thickness of cover layers particularly when a weak layer is overlying a stronger one, has the most significant influence on the minimum tunnel support pressure.

Han and Liu (2016) investigated the failure mechanisms of circular cast-iron tunnels in saturated soil subjected to medium internal blast loading and found that the damage of tunnel lining was a result of internal blast loading as well as dynamic interaction between tunnel lining and saturated soil.

Nikadat and Marji (2016) evaluated the effects of joints spacing and joints orientation by using a hybridized indirect boundary element method and found that that the tensile and compressive tangential stresses at the boundary of the circular tunnel increase by reduction in the joint spacing, and by increase the dip joint angle the tensile stress in the tunnel roof decreases.

Li *et al.* (2016a) studied the mechanism of macro failure and micro fracture of local nearly horizontal stratum in super-large section and deep buried tunnel and proposed a simple analytical, economical and efficient approach.

Li *et al.* (2016b) studied water flow characteristics after inrushing in process of karst tunnel excavation, using numerical simulations for five case studies and obtained important results to ensure safe tunnel construction.

Yoo (2016) studied the deformation behavior of tunnels crossing a weak zone with emphasis on the spatial characteristics of the weak zone (such as the strike and dip angle) and concluded that proper interpretation of the monitoring data can provide early warning and also the orientation and the extent of the weak zone.

Sevim (2013) investigated the earthquake response of the Arhavi Highway Tunnel using a 3D finite element model and found that the displacement and stress results were found to be in the allowable level of the concrete material.

Al-Omari *et al.* (2016) successfully used both experimental modeling and finite element analysis to investigate the behavior of piled rafts overlying a tunnel in a sandy soil.

Yang *et al.* (2016) investigated the effect of the soil's dilatancy coefficient on the collapse mechanism of a tunnel roof in homogeneous and layered soils considering the influences of nonlinearity and non-associated flow rule.

Nawel and Salah (2015) studied the interaction effects between two real parallel tunnels by using 3-D Finite Element modeling and analyses.

Liu *et al.* (2015) investigated by finite element numerical simulation a shallow-buried bilateral bias twin-tube tunnel surrounded by rock and subjected to seismic forces, considering rupture angles, the failure mode of the tunnel and the distribution of surrounding rock relaxation pressure and provided recommendations for the rock reinforcement.

Mazek (2014) investigated the limitations of the parameters used in the "Surface Displacement Equation" (SDE), and using the Finite Element Analysis at different sand soil densities showed that the different sand soil densities neglected in the SDE have a significant influence on the surface displacement due to tunneling in cohesionless soil.

Do *et al.* (2014) performed 2D numerical investigations of the interaction in twin tunnels and studied the effect of segment joints and tunnel distance and found that the critical influence distance between them is about two tunnel diameters.

Fattah *et al.* (2015) studied the dynamic response of a lined concrete tunnel with transmitting boundaries, investigated the validity of the transmitting boundaries of this soil-structure interaction problem and also found that the results present significant differences when earthquake is applied as a base motion or a pressure load is applied at the surface ground.

Abdelrahim *et al.* (2015) studied the twin tunnel configuration for Greater Cairo metro line No. 4, performed the numerical analysis by using two-dimensional models, and identified the suitable clear distance between the twin tunnels according to internal forces and displacements in tunnels, which has a major effect on soil movement and internal forces in tunnel lining.

The four-track surface railway is located in Sohag city in Upper Egypt and the tunnel is constructed as an underground pedestrian tunnel connecting the automated bakery area in the West Sohag district with the area of Assiut-Sohag Road at the eastern district, where earlier the pedestrians were prohibited from the tracks on the railway, and it was needed to be constructed in order to prevent accidents.

The pedestrian tunnel has a length of 28 m, while its cross-section is circular of 5m internal diameter and reinforced concrete thickness of 400 mm.

The weather in Upper Egypt is a very continental climate where rainfall is rare, so the soil under the railway sleepers is almost dry all the year. However sudden storms sometimes cause devastating flash floods. Heavy rainfall and soil exposure to drying lead to soil with different water content throughout the year.

The pedestrian tunnel and the soil block around the tunnel are modeled in 3D by the FEM and are studied under the vibrations induced by the moving trains on the four-track surface railway for different soil water contents and the effects of the soil water content on the dynamic behavior of the tunnel and the surrounding soil are demonstrated.

2. Soil properties for different water contents

The soil is an uncontrolled medium because of the effect of natural factors, where the most effective parameter in the

Table 1 Soil specifications for different water contents (Abdelrahim *et al.* 2017)

Shear strength parameters and other properties	Water Content 1%	Water Content 15%	Water Content 30%
Cohesion (kg/cm^2), c	0.03	0.23	0.08
Angle of internal friction (degrees), φ	22	12	7
Bulk density of cohesive soil (t/m^3), γ_b	1.52	1.73	1.97
Poisson's Ratio, ν	0.37	0.44	0.47
Modulus of Elasticity (t/m^2), E	1100	910	730

soil is the water, and changing of the water content in soil, changes the soil properties and the bearing and dynamic soil properties under different kinds of loads.

Herein three different water contents were checked to show the effect of the change of the soil water content on the soil and consequently on the pedestrian RC tunnel as a result of the soil structure interaction between the soil and the tunnel.

The particle size distribution curve of the soil showed that the soil is 71% silt, 24% clay and 5% sand, the soil is classified as clayey silt and medium plasticity silt (MI); the consistency limits were determined by Casagrande's method and the results can be summarized as follows: liquid limit = 48%, plastic limit = 29%, plasticity index = 19%, specific gravity Gs = 2.56, dry density = 1.505 t/m^3 (Abdelrahim *et al.* 2017).

The shear strength parameters (cohesion, c and angle of internal friction, φ), Poisson's Ratio, ν and Modulus of Elasticity, E of the soil were determined for different water contents using direct shear tests, and triaxial compression tests and the results obtained are shown in Table 1 (Abdelrahim *et al.* 2017).

The cohesion (c) of the above clayey silt is found to increase with increasing water content to a certain level, after which it decreases. The angle of internal friction (φ) for clayey silt is found generally to decrease with increasing water content. Similar observations have been made e.g., by Wells and Treesuwan (1978), Al-Shayea (2001), Dong *et al.* (2011), and Bashar *et al.* (2015).

3. Model description

Fig. 1 shows the description of the model used in the study. Fig. 1(a) shows the longitudinal section of the tunnel with the details of the four railway lines (tracks) and the cross section cross section of the tunnel. The depth of the tunnel crown is 1 m. The infill under the railway above the tunnel crown should be not less than 1 m in order to absorb the vibrations induced by the moving trains. The 4 tracks (lines 1, 2, 3, and 4) of the quadruple-track (four-track) surface railway (over the tunnel) are also shown in Fig. 1(a). Four different dynamic load cases induced by the moving trains were studied for three different water contents (1%, 15% and 30%) in the soil around the tunnel and under the railway. These train-induced dynamic load cases were: only one outer track (at the edge near the start: line 1) is occupied with moving train, two inner (central) tracks (lines 4 and 3) are occupied with moving trains, two outer tracks (at the edges: lines 4 and 1) are occupied with moving trains, and all 4 tracks (lines 1, 2, 3, and 4) are occupied with moving trains.

Fig. 1(b) represents the 3D FEM model of the soil block and pedestrian tunnel, used in the SAP2000, where the soil is represented by solid elements, the tunnel is represented by shell elements, and the railway is represented by frame elements (for each railway track, two frame elements). The 3D FEM model of the soil block with length of 50 m, depth of 25 m and width of 28 m was represented by solid elements in SAP2000; the boundary conditions under the soil block are hinged supports and around the block are roller supports. The 3D FEM model of the reinforced concrete pedestrian tunnel (under the railway), with length of 28 m, circular cross-section with internal diameter of 5 m and RC thickness of 400 mm, was represented by shell elements in SAP2000.

Fig. 1(c) represents the cross section of the soil block with the circular pedestrian RC tunnel (all dimensions are in m) where the depth of the tunnel crown is 1 m.

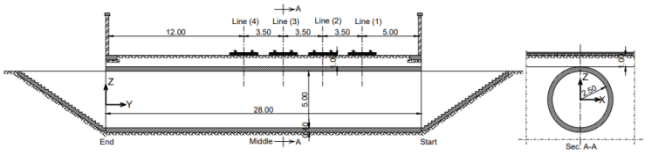

(a) Tunnel longitudinal section with the details of the railway lines (tracks) and cross section (dimensions in m)

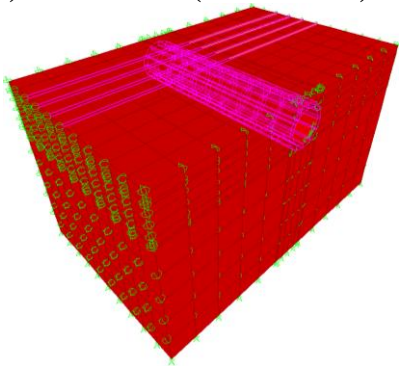

(b) 3D FEM model of the soil block and pedestrian tunnel with boundary conditions

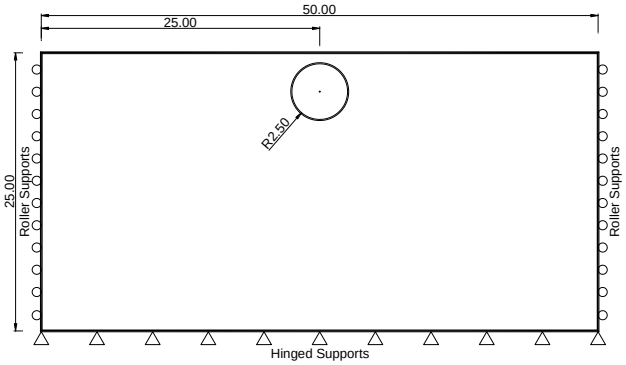

(c) Cross section of the soil block (dimensions in m)

Fig. 1 Description of the model

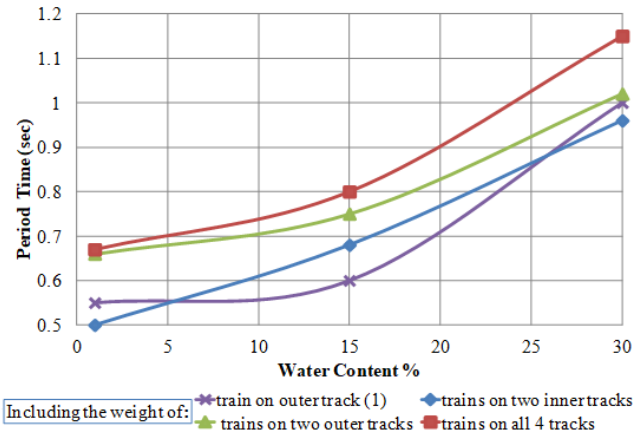

Fig. 2 Natural period time for different soil water contents

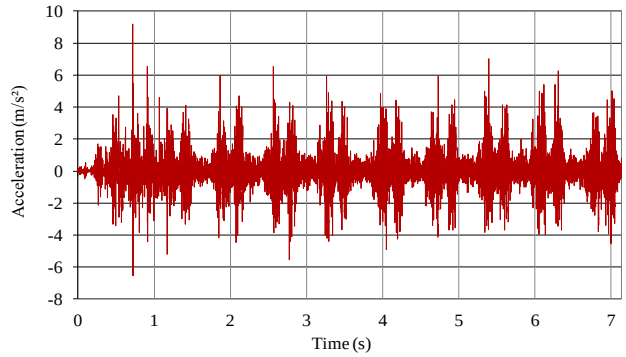

(a) Acceleration signals for a train

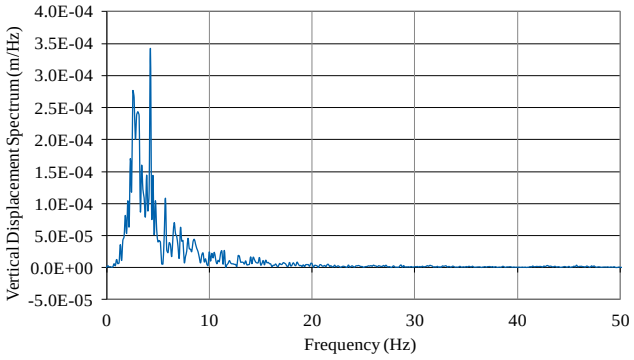

(b) Vertical Displacement Spectrum

Fig. 3 Measurements on the track ballast for a current train (Picoux 2002)

4. Natural period of the model for different soil water contents

Fig. 2 represents the natural period of the model including the train weight for different occupied tracks cases and soil water contents. The four railway tracks (lines) were shown in Fig. 1(a). The natural period time in outer track (1) and two inner tracks (lines 4 and 3) occupied cases, is the lower in time, however increasing water content increases the period time. The two outer tracks (lines 4 and 1) and all 4 tracks (lines 4, 3, 2 and 1) occupied cases give the higher period time than the rest cases. The maximum period time takes place in the all 4 tracks occupied case and this natural period time increases when the soil water content increases, which means that the heavier weight case with the higher water content, gives the higher natural period time.

5. Moving train accelerogram

Picoux (2002), and Picoux and Le Houédec (2005) in order to diagnose and predict the vibration from railway trains near the track, successfully developed a prediction model and also performed in situ measurements with the aim of the validation of their proposed model.

A real accelerogram of a moving train is presented in Fig. 3(a) (Picoux 2002). The measurements for 7 secs of the acceleration signals were on track ballast for a current train (heavy locomotive and many current carriages) moving at 135 km/h (Picoux 2002). The vertical displacement spectrum (m/Hz) calculated by double integration and Fourier transform is shown in Fig. 3(b) (Picoux 2002).

6. Dynamic load cases induced by the moving trains

The 4 tracks (lines 1, 2, 3, and 4) of the quadruple-track (four-track) surface railway (over the tunnel) are shown in Fig. 1(a). Four different dynamic load cases induced by the moving trains were studied for three different water contents (1%, 15% and 30%) in the soil around the tunnel and under the railway. These train-induced dynamic load cases were: only one outer track (at the edge near the start: line 1) is occupied with moving train, two inner (central) tracks (lines 4 and 3) are occupied with moving trains, two outer tracks (at the edges: lines 4 and 1) are occupied with moving trains, and all 4 tracks (lines 1, 2, 3, and 4) are occupied with moving trains.

The dynamic responses of the tunnel and the soil are presented by the maximum displacements and stresses in the tunnel (shell elements) and by the maximum stresses in the soil (solid elements), under the aforementioned four dynamic load cases and for the three soil water contents (1%, 15% and 30%).

6.1 Moving train on outer track (1)

Fig. 4 represents the maximum response of the tunnel and the soil for one train moving on outer track (1) over the tunnel (see Fig. 1(a): line 1) with different water contents (1%, 15% and 30%) in the soil around the tunnel.

Fig. 4(a) shows the tunnel displacements at the top and bottom of the tunnel along the start (0), middle (14 m) and end (28 m) of the tunnel length (see Fig. 1(a)) for different soil water contents; the horizontal X displacement at the start of the tunnel length, increases at the top of the tunnel by 2 times, and at the bottom of the tunnel by 1.6 times when the water content increases from 1% to 30%; the horizontal X displacement at the middle of the tunnel length, increases at the top of the tunnel by 1.9 times, and at the bottom of the tunnel by 1.7 times when the water content increases from 1% to 30%; the horizontal Y displacement at the start of the tunnel length, increases at the bottom of the tunnel by 1.15 times when the water

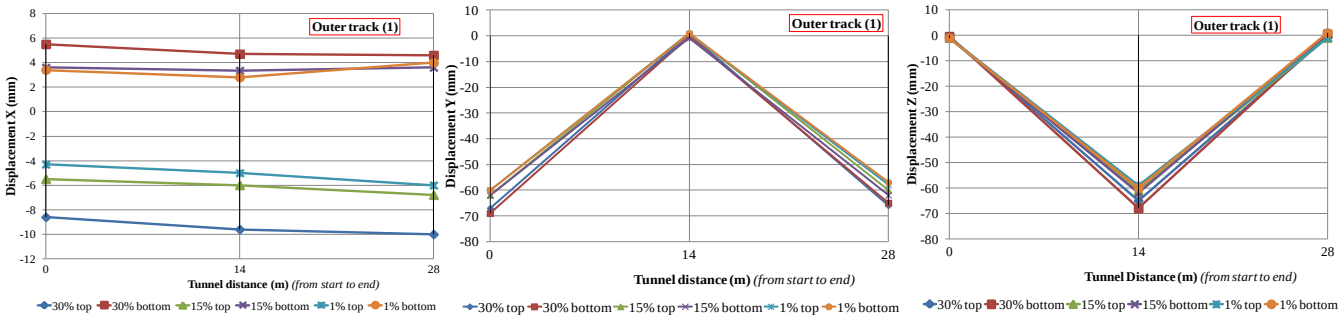

UX UY UZ

(a) Displacements (in X, Y, Z directions) at the top and bottom points of the tunnel

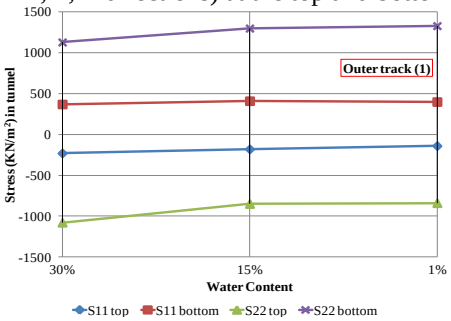

(b) Stresses at the top and bottom of the tunnel at the middle of the tunnel length

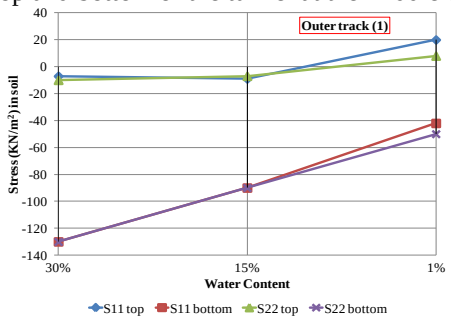

(c) Stresses in the soil at the middle of the tunnel length

Fig. 4 Displacements and stresses in the tunnel and stresses in the soil–Moving train on outer track (1)

content increases from 1% to 30%; the vertical Z displacement at the middle of the tunnel length, increases at the bottom of the tunnel by 1.13 times when the water content increases from 1% to 30%, and at 30% equals -68 mm.

Fig. 4(b) shows the tunnel stresses at the top and bottom of the tunnel, the stresses at top are compressive and the stresses at bottom are tensile and the higher the moisture contents of the soil, the higher stresses at the top of the reinforced concrete tunnel and the lower stresses at the bottom on the reinforced concrete tunnel.

Fig. 4(c) shows the stresses in the soil at top of the tunnel and under it; compressive soil stresses increase by about 3 times at the bottom of the tunnel when water content change from 1% to 30% while at the top of the tunnel the soil stresses are tensile for water content 1% and equals 20 KN/m^2 which indicate failure of the soil around the top of tunnel and afterwards become compressive for soil water contents 15% and 30%.

Fig. 5 shows the maximum stress contours in the tunnel and in the center of the soil block for one train moving on outer track (1) over the tunnel with different soil water contents (1%, 15% and 30%).

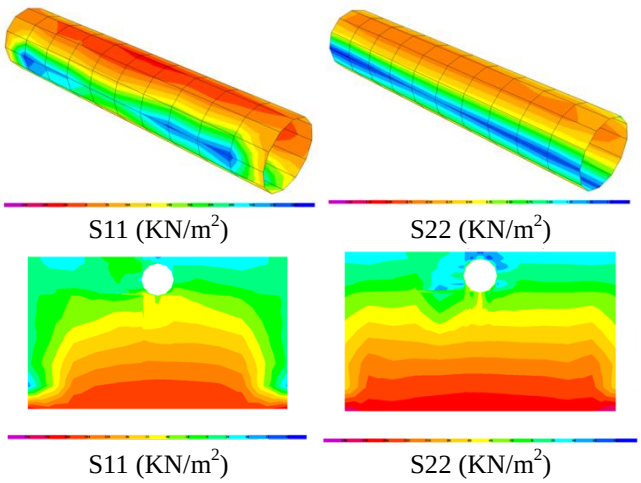

S11 (KN/m^2) S22 (KN/m^2)

S11 (KN/m^2) S22 (KN/m^2)

(a) Water Content 1%

Fig. 5 Stress contours in the tunnel and soil - Moving train on outer track (1)

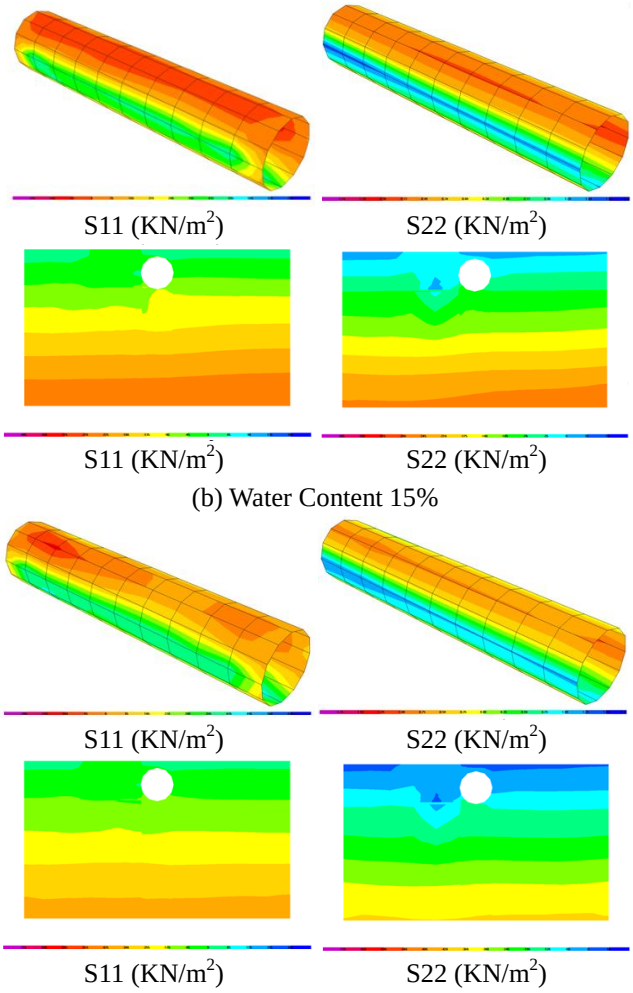

(b) Water Content 15%

(c) Water Content 30%

Fig. 5 Continued

6.2 Moving trains on the two inner (central) tracks

Fig. 6 displays the maximum response of the tunnel and the soil for trains moving on the two inner (central) tracks (see Fig. 1(a): lines 4 and 3) over the tunnel with different soil water contents (1%, 15% and 30%).

Fig. 6(a) shows the displacements at the top and bottom of the tunnel along the start (0), middle (14 m) and end (28 m) of the tunnel length (see Fig. 1(a)) for different soil water contents; the horizontal X displacement at the start of the tunnel length, increases at the top of the tunnel by 1.5 times and at the bottom of the tunnel by 1.1 times when the water content increases from 1% to 30%; the horizontal X displacement at the middle of the tunnel length, increases at the top of the tunnel by 1.4 times and at the bottom of the tunnel by 1.1 times when the water content increases from 1% to 30%; the horizontal Y displacement at the start of the tunnel length, increases at the bottom of the tunnel by 1.13 times when the water content increases from 1% to 30%; the vertical Z displacement at the middle of the tunnel length, increases at the bottom of the tunnel by almost 1.1 times when the water content increases from 1% to 30% and at 30% equals -68 mm.

Fig. 6(b) represents the maximum tunnel stresses at the top and bottom of the RC tunnel for different soil water content values; the stresses at top are compressive and the stresses at bottom are tensile and the higher the moisture contents of the soil, the higher stresses at the top of the reinforced concrete tunnel and the lower stresses at the bottom on the reinforced concrete tunnel.

Fig. 6(c) represents the stresses in the soil at top and bottom of the tunnel, the stresses at bottom are all in compression state, but tension appears in the soil at the top of the tunnel and equals to 1 KN/m^2 for 15% water content and 7.4 KN/m^2 for 1% water content which indicate the failure of the soil around the top of tunnel, while afterwards compression takes place in the soil at the top of the tunnel for soil water content 30%.

Fig. 7 shows the maximum stress contours in the tunnel and in the center of the soil block for trains moving on the two inner (central) tracks over the tunnel with different soil water contents (1%, 15% and 30%).

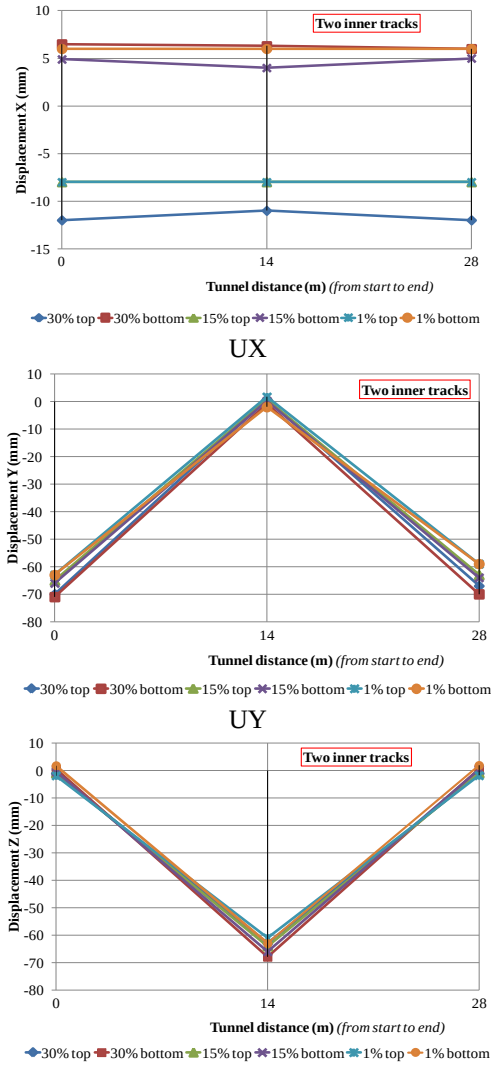

(a) Displacements (in X, Y, Z directions) at the top and bottom points of the tunnel

Fig. 6 Displacements and stresses in the tunnel and stresses in the soil - Moving trains on two inner (central) tracks

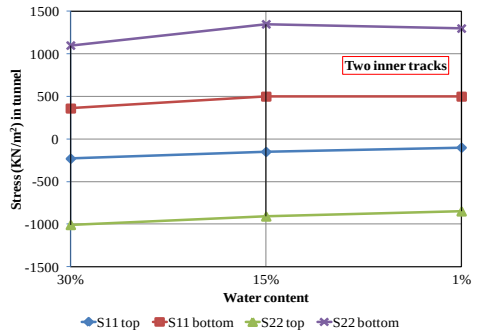

(b) Stresses at the top and bottom of the tunnel at the middle of the tunnel length

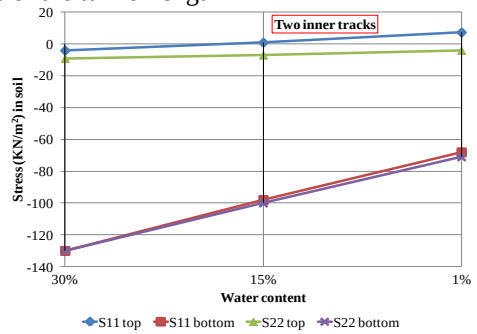

(c) Stresses in the soil at the middle of the tunnel length

Fig. 6 Continued

6.3 Moving trains on the two outer tracks

Fig. 8 represents the maximum response of the tunnel and the soil for trains moving on the two outer tracks (see Fig. 1(a: lines 4 and 1) over the tunnel with different soil water contents (1%, 15% and 30%) in the soil around the tunnel.

Fig. 8(a shows the displacements at the top and bottom of the tunnel along the start (0), middle (14 m) and end (28 m) of the tunnel length (see Fig. 1(a) for different soil water contents; the horizontal X displacement at the start of the tunnel length, increases at the top of the tunnel by 1.5 times and at the bottom of the tunnel by 1.1 times when the water content increases from 1% to 30%; the horizontal X displacement at the middle of the tunnel length, increases at the top of the tunnel by 1.6 times and at the bottom of the tunnel by 1.2 times when the water content increases from 1% to 30%; the horizontal Y displacement at the start of the tunnel length, increases at the bottom of the tunnel by 1.1 times when the water content increases from 1% to 30%; the vertical Z displacement at the middle of the tunnel length, increases at the bottom of the tunnel by almost 1.1 times when the water content increases from 1% to 30% and at 30% equals -68 mm.

Fig. 8(b) represents the maximum tunnel stresses at the top and bottom of the reinforced concrete tunnel for different soil water content; the stresses at top are compressive and the stresses at bottom are tensile and the higher the moisture contents of the soil, the higher stresses at the top of the RC tunnel and the lower stresses at the bottom on the RC tunnel.

Fig. 8(c) represents the stresses in soil at top and bottom of the tunnel, the stresses at bottom are all

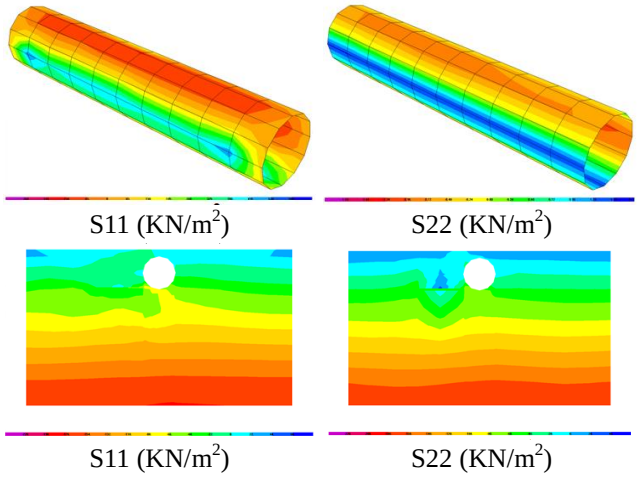

(a) Water Content 1%

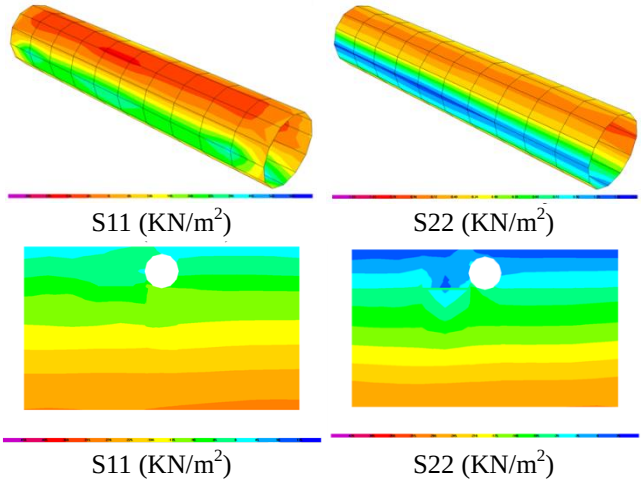

(b) Water Content 15%

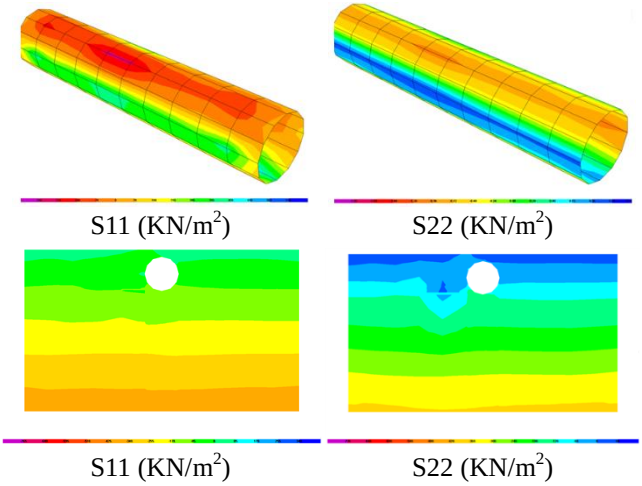

(c) Water Content 30%

Fig. 7 Stress contours in tunnel and soil - Moving trains on two inner (central) tracks

compression state, but tension appears in the soil at the top of the tunnel and equals to S11=21.7 KN/m^2 for 30% water content, S11=14.9 KN/m^2 for 15% water content and 19.9 KN/m^2 for 1% water content which indicate failure of the soil around the top of tunnel; while at the bottom of the tunnel the compressive soil stress increase in 30% water

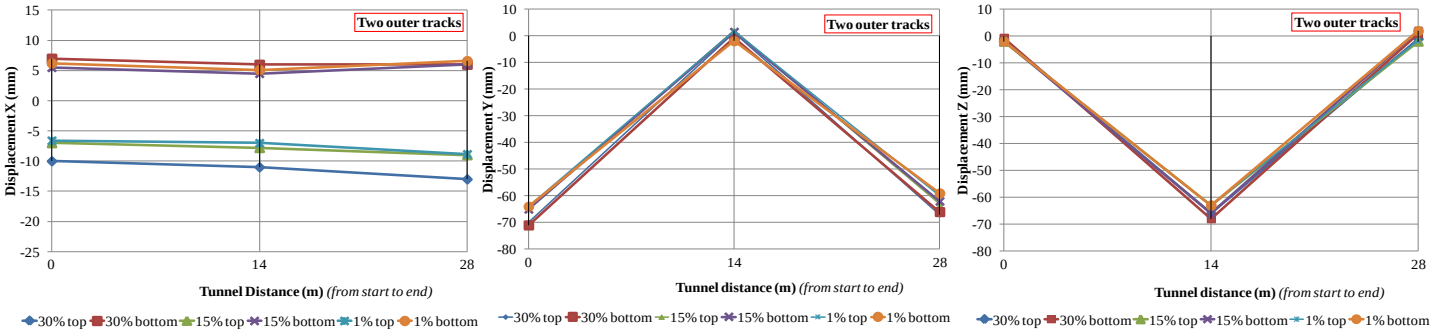

UX UY UZ

(a) Displacements (in X, Y, Z directions) at the top and bottom points of the tunnel

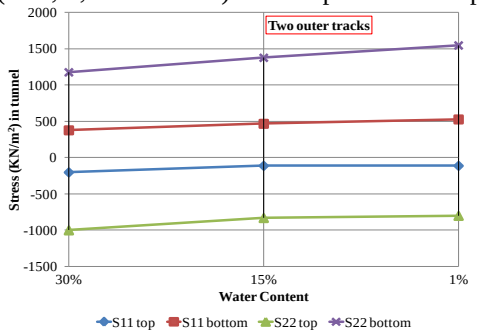

(b) Stresses at the top and bottom of the tunnel at the middle of the tunnel length

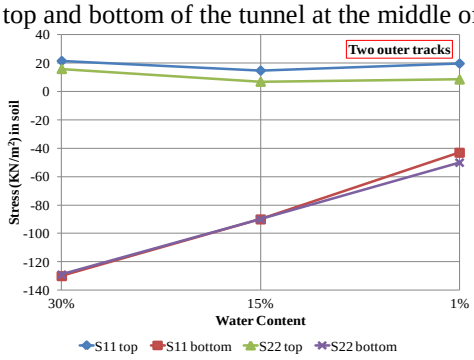

(c) Stresses in the soil at the middle of the tunnel length

Fig. 8 Displacements and stresses in the tunnel and stresses in the soil-Moving trains on two outer tracks

content by approximately 3 times than in 1% water content.

Fig. 9 shows the maximum stress contours in the tunnel and in the center of the soil block for trains moving on the two outer tracks over the tunnel with different soil water contents (1%, 15% and 30%).

6.4 Moving trains on all 4 tracks

Fig. 10 represents the maximum response of the tunnel and the soil for trains moving on all 4 tracks (see Fig. 1(a): lines 1, 2, 3 and 4) over the tunnel for different water contents (1%, 15% and 30%) in the soil around the tunnel. Fig. 10(a) shows the displacements at the top and bottom of the tunnel along the start (0), middle (14 m) and end (28 m) of the tunnel length (see Fig. 1(a)) for different soil water contents; the horizontal X displacement at the start of the tunnel length, increases at the top of the tunnel by 1.1 times and decreases at the bottom of the tunnel by 0.8 times when the water content increases from 1% to 30%; the horizontal X displacement at the middle of the tunnel length, increases at the top of the tunnel by 1.25 times and at the bottom almost does not change when the water content increases

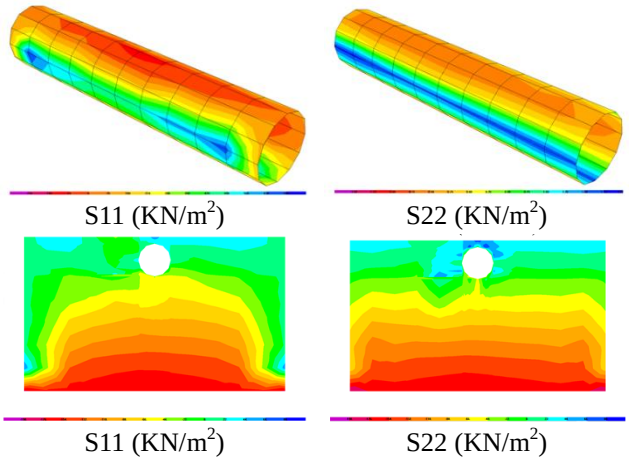

(a) Water Content 1%

Fig. 9 Stress contours in tunnel and soil - Moving trains on two outer tracks

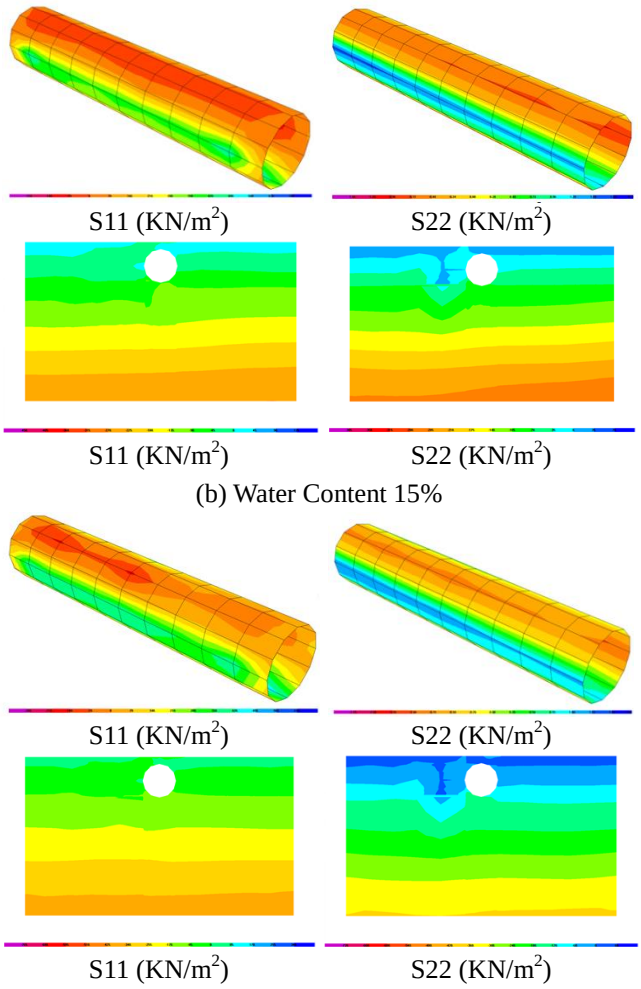

(b) Water Content 15%

(c) Water Content 30%

Fig. 9 Continued

from 1% to 30%; the horizontal Y displacement at the start of the tunnel length, increases at the bottom of the tunnel by 1.04 times when the water content increases from 1% to 30%; the vertical Z displacement at the middle of the tunnel length, increases at the bottom of the tunnel by almost 1.06 times when the water content increases from 1% to 30% and at 30% equals -71 mm.

Fig. 10(b) represents the maximum tunnel stresses at the top and bottom of the reinforced concrete tunnel for different soil water content values; the stresses at top are compressive and the stresses at bottom are tensile and the higher the moisture contents of the soil, the higher stresses at the top of the RC reinforced concrete tunnel and the lower stresses at the bottom of the RC tunnel.

Fig. 10(c) represents the stresses in soil at top and bottom of the tunnel, the stresses at bottom are all compression state, but tension appears in the soil at the top of the tunnel and equals to S11=1.5 KN/m^2 for 30% water content, S11=6.8 KN/m^2 for 15% water content and 12.6 KN/m^2 for 1% water content which indicate the failure of the soil around the top of tunnel; while at the bottom of the tunnel the compressive soil stresses increase by approximately 2 times in 30% water content than in 1% water content.

Fig. 11 shows the maximum stress contours in the tunnel and in the center of the soil block for trains moving on all 4 tracks over the tunnel with different soil water contents (1%, 15% and 30%).

6.5 Comparison of results

In the following figures some comparisons of selected

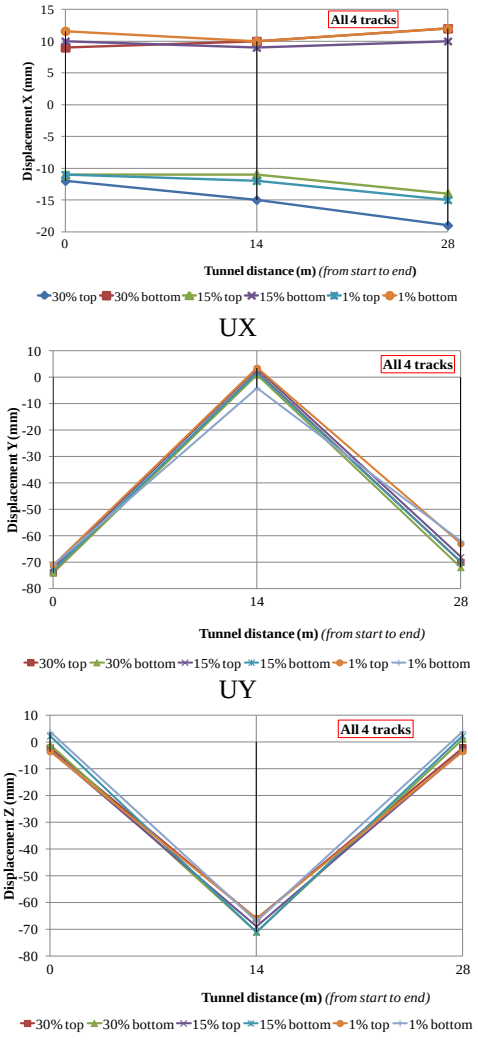

(a) Displacements (in X, Y, Z directions) at the top and bottom points of the tunnel

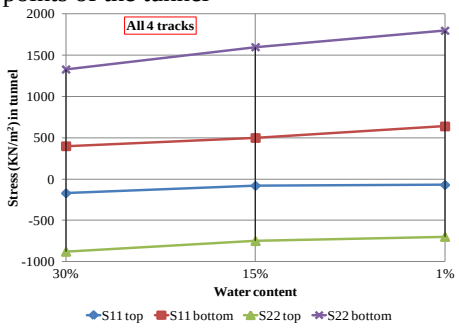

(b) Stresses at the top and bottom of the tunnel at the middle of the tunnel length

Fig. 10 Displacements and stresses in the tunnel and stresses in the soil-Moving trains on all 4 tracks

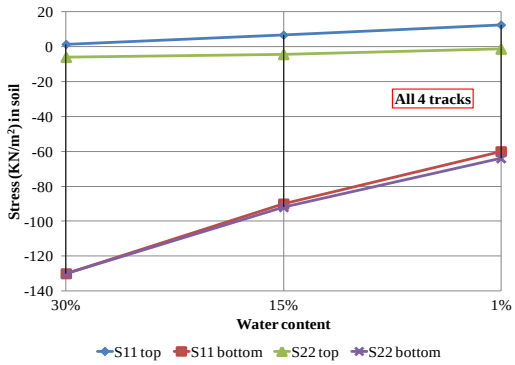

(c) Stresses in the soil at the middle of the tunnel length

Fig. 10 Continued

results are depicted for the four train-induced dynamic load cases: one train moving on outer track (1), trains moving on the two inner (central) tracks (lines 4 and 3), trains moving on the two outer tracks (at the edges: lines 4 and 1), and trains moving on all 4 tracks (lines 1, 2, 3, and 4) over the tunnel with different water contents (1%, 15% and 30%) in the soil around the tunnel.

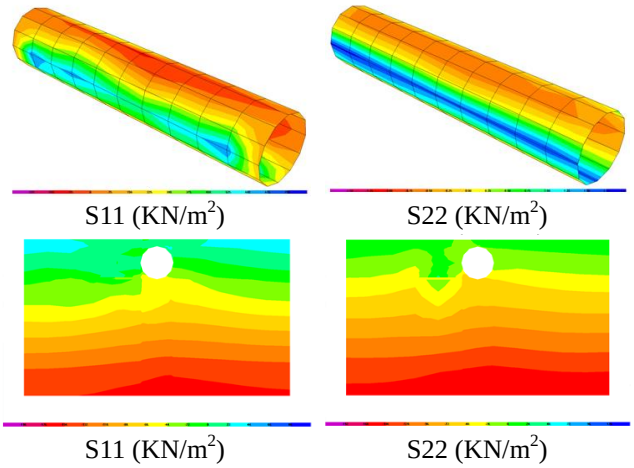

(a) Water Content 1%

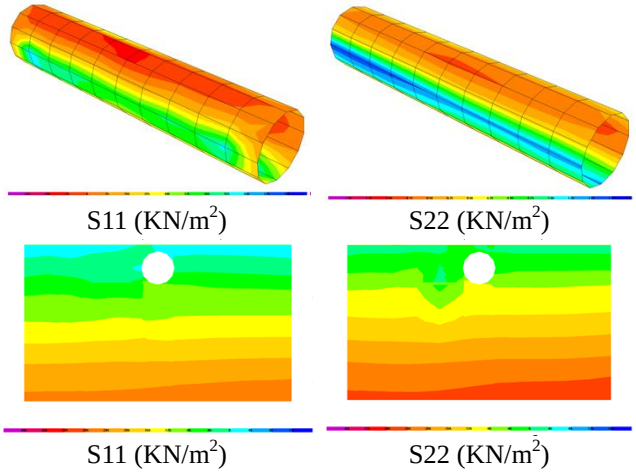

(b) Water Content 15%

Fig. 11 Stress contours in tunnel and soil-Moving trains on all 4 tracks

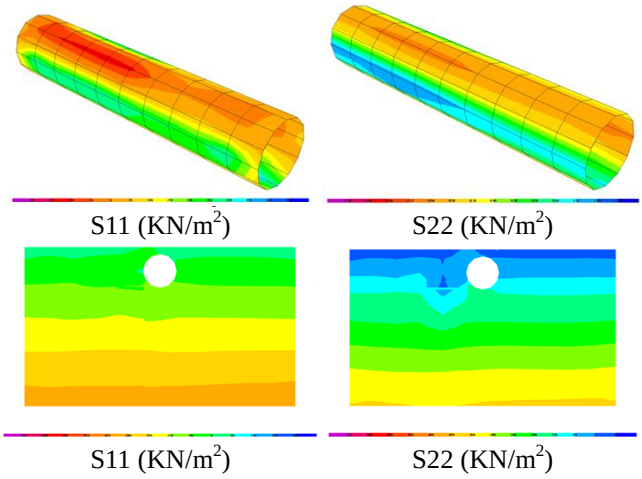

(c) Water Content 30%

Fig. 11 Continued

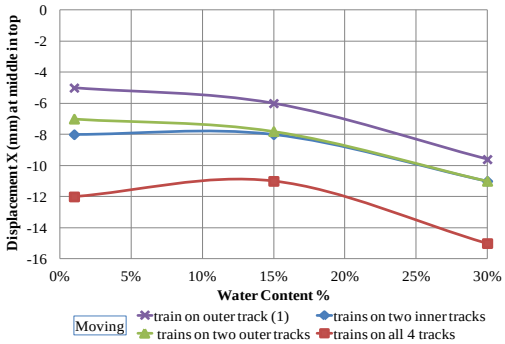

Fig. 12 Displacements in X direction in the top of the tunnel at the middle of the tunnel length

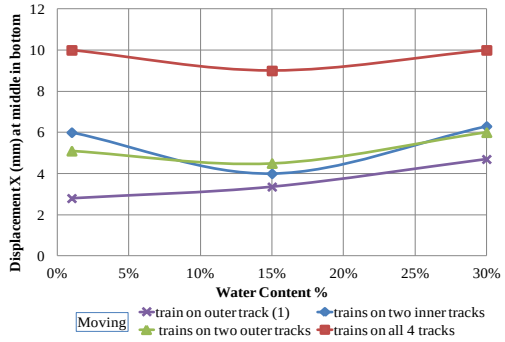

Fig. 13 Displacements in X direction in the bottom of the tunnel at the middle of the tunnel length

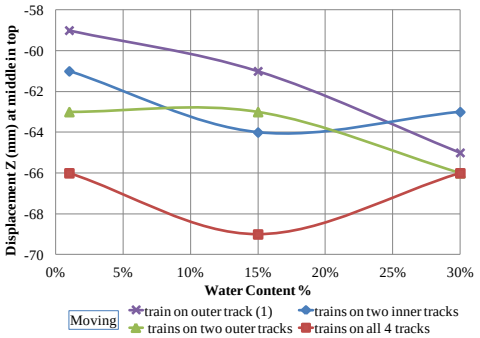

Fig. 14 Displacements in Z direction in the top of the tunnel at the middle of the tunnel length

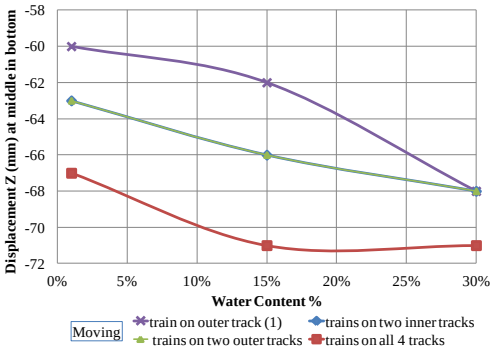

Fig. 15 Displacements in Z direction in the bottom of the tunnel at the middle of the tunnel length

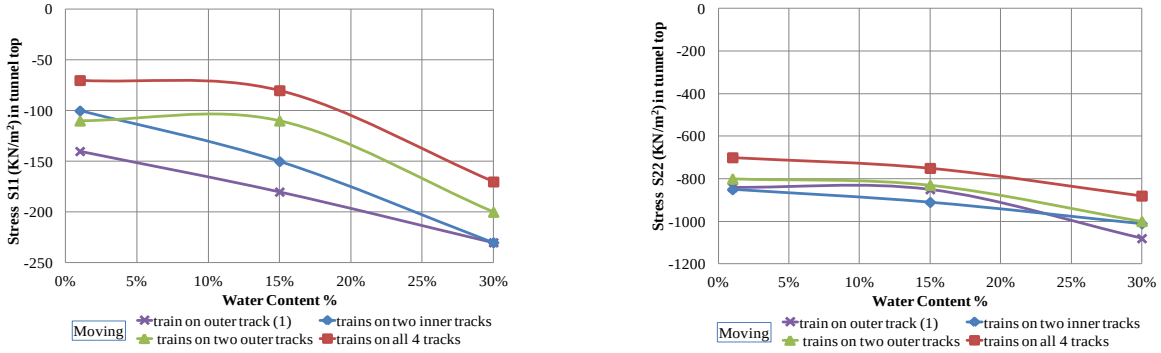

Fig. 16 Stresses at the top of the tunnel at the middle of the tunnel length

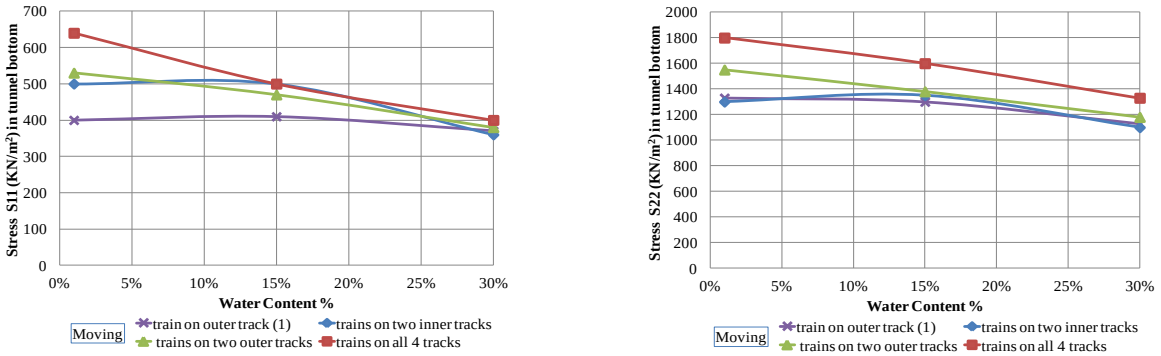

Fig. 17 Stresses at the bottom of the tunnel at the middle of the tunnel length

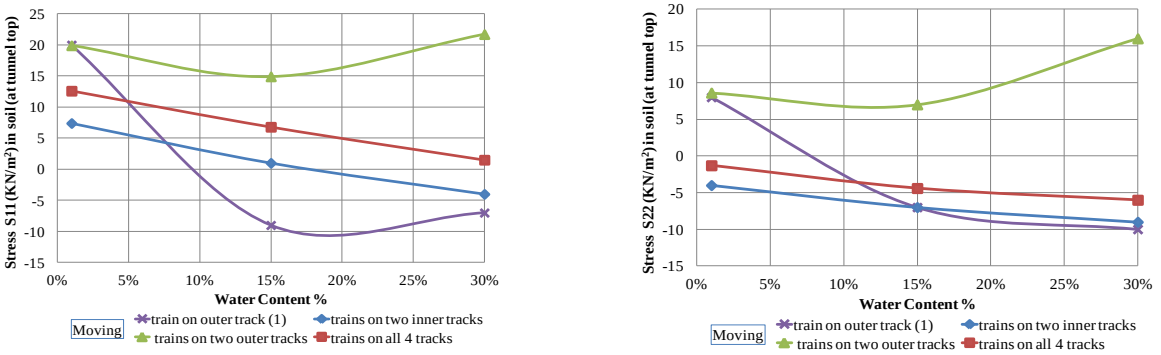

Fig. 18 Soil stresses at the top of the tunnel at the middle of the tunnel length

Figs. 12 and 13 show the horizontal X displacement at the top and at the bottom of the tunnel respectively, at the middle of the tunnel length for the four dynamic load cases induced by moving trains and for three soil water contents (1%, 15% and 30%).

Figs. 14 and 15 show the vertical Z displacement at the top and at the bottom of the tunnel respectively, at the middle of the tunnel length for the four dynamic load cases

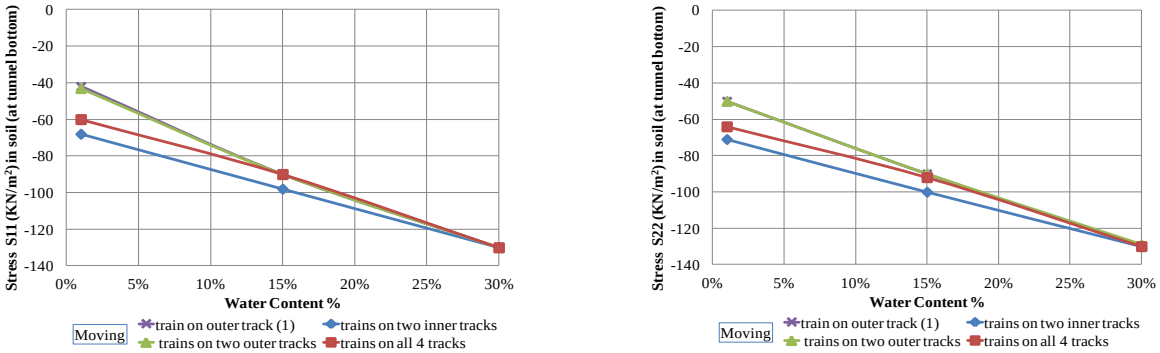

Fig. 19 Soil stresses at the bottom of the tunnel at the middle of the tunnel length

induced by moving trains and for three soil water contents (1%, 15% and 30%).

Figs. 16 and 17 show the stresses at the top and at the bottom of the tunnel respectively, at the middle of the tunnel length for the four dynamic load cases induced by moving trains and for three soil water contents (1%, 15% and 30%).

Figs. 18 and 19 show the soil stresses at the top and at the bottom of the tunnel respectively, at the middle of the tunnel length for the four dynamic load cases induced by moving trains and for three soil water contents (1%, 15% and 30%).

7. Conclusions

A reinforced concrete pedestrian tunnel was planned to be constructed in Sohag, Egypt, under the four-track surface railway. The nature of the soil as an uncontrolled media (because of the natural resources which can affect it, like the water table, rainfall, etc.) must be taken into consideration in the design of infrastructure works, thus for different water contents of the soil around the tunnel body, the responses of the tunnel and soil were studied under four different dynamic load cases due to moving trains on the railway tracks and the following conclusions were drawn and should be taken into consideration in the tunnel design:

• The natural period of the model increases as the water content increases in the soil.

• Vertical displacement in the bottom of the tunnel increases as water content increases in the soil.

• Vertical displacements in the top and the bottom of the tunnel are bigger when trains are moving on all four railway tracks.

• Stresses at the top of the tunnel are compressive and increase as the soil water content increases.

• Stresses at the bottom of the tunnel are tensile and are bigger when trains are moving on all four railway tracks. The tensile stresses at the bottom of the tunnel decrease as the soil water content increases. The lower the water contents in the soil, the greater the stresses at the bottom of the reinforced concrete tunnel.

• Soil stresses at the top of the tunnel become tensile which indicate the failure of the soil around the top of tunnel and are bigger when trains are moving on the two outer tracks.

• Soil stresses at the bottom of the tunnel are compressive and are a little bigger when trains are moving on the two inner (central) tracks. The compressive soil stresses at the bottom of the tunnel increase as the soil water content increases.

• The dynamic effect of the moving trains increases the danger of soil liquefaction, especially in cases of increased soil water content, which is characterized by increased settlement.

• A drain system is necessary to protect the soil under the railway and around the tunnel from an increase of the soil water content.

Acknowledgements

The authors would like to express their gratitude to Dr. Benoit Picoux (Assoc. Professor, Department of Civil Engineering and Durability, University of Limoges, France) for providing train accelerograms from measurements on a railway track for a current train.

References

Abdelrahim, H.H.A., Enieb, M., Abdelmoamen Khalil, A. and Ahmed, A.S.H. (2015), "Twin tunnel configuration for Greater Cairo metro line No. 4", *Comput. Geotech.*, **68**, 66-77.

Abdelrahim, H.H.A., Yehia, K., Ahmed, A. and El Sarif, W.M. (2017), "Properties affecting the compression capacity of helical piles in cohesive soils", *Minia J. Eng. Technol.*, **36**(1), 32-46.

Aksoy, C.O., Uyar, G.G., Posluk, E., Ogul, K., Topal, I. and Kucuk, K. (2016), "Non-deformable support system application at tunnel-34 of Ankara-Istanbul high speed railway project", *Struct. Eng. Mech.*, **58(**5), 869-886.

Al-Omari, R.R., Al-Azzawi, A.A. and AlAbbas, K.A. (2016), "Behavior of piled rafts overlying a tunnel in sandy soil", *Geomech. Eng.*, **10**(5), 599-615.

Al-Shayea, N.A. (2001), "The combined effect of clay and moisture content on the behavior of remolded unsaturated soils", *Eng. Geol.*, **62**(4), 319-342.

Bashar, M., Zhou, Y. and Jun, L. (2015), "Effect of soil strength and soil physical properties on performance of tillage machines", *J. Earth Sci. Eng.*, **5**, 251-255.

Cui, S., Liu, P., Wang, X., Cao, Y. and Ye, Y. (2017), "Experimental study on deformation of concrete for shotcrete use in high geothermal tunnel environments", *Comput. Concrete*, **19**(5), 443-449.

Ding, W.Q., Peng, Y.C., Yan, Z.G., Shen, B.W., Zhu, H.H. and Wei, X.X. (2013), "Full-scale testing and modeling of the mechanical behavior of shield TBM tunnel joints", *Struct. Eng. Mech.*, **45**(3), 337-354.

Ding, Z., Wei, X.J. and Wei, G. (2017), "Prediction methods on tunnel-excavation induced surface settlement around adjacent building", *Geomech. Eng.*, **12**(2), 185-195.

Do, N.A., Dias, D., Oreste, P. and Djeran-Maigre, I. (2014), "2D numerical investigations of twin tunnel interaction", *Geomech. Eng.*, **6**(3), 263-275.

Dong, Y., Wu, Y., Yin, J., Wang, Y. and Gou, S. (2011), "Investigation of soil shear-strength parameters and prediction of the collapse of gully walls in the black Soil region of Northeastern China", *Phys. Geogr.*, **32**(2), 161-178.

Fattah, M.Y., Hamoo, M.J. and Dawood, S.H. (2015), "Dynamic response of a lined tunnel with transmitting boundaries", *Earthq. Struct.*, **8**(1), 275-304.

Han, J.S., Won, B., Park, W.S. and Ko, J.H. (2016), "Transient response analysis by model order reduction of a Mokpo-Jeju submerged floating tunnel under seismic excitations", *Struct. Eng. Mech.*, **57**(5), 921-936.

Han, Y. and Liu, H. (2016), "Failure of circular tunnel in saturated soil subjected to internal blast loading", *Geomech. Eng.*, **11**(3), 421-438.

Jafarnia, M. and Varzaghani, M.I. (2016), "Effect of near field earthquake on the monuments adjacent to underground tunnels using hybrid FEA-ANN technique", *Earthq. Struct.*, **10**(4), 757-768.

Khezri, N., Mohamad, H. and Fatahi, B. (2016), "Stability assessment of tunnel face in a layered soil using upper bound theorem of limit analysis", *Geomech. Eng.*, **11**(4), 471-492.

Li, S.C., Wang, J.H., Chen, W.Z., Li, L.P., Zhang, Q.Q. and He, P. (2016a), "Study on mechanism of macro failure and micro fracture of local nearly horizontal stratum in super-large section and deep buried tunnel", *Geomech. Eng.*, **11**(2), 253-267.

Li, S.C., Wu, J., Xu, Z.H., Li, L.P., Huang, X., Xue, Y.G. and Wang, Z.C. (2016b), "Numerical analysis of water flow characteristics after inrushing from the tunnel floor in process of karst tunnel excavation", *Geomech. Eng.*, **10**(4), 471-526.

Liu, X.R., Li, D.L., Wang, J.B. and Wang, Z. (2015), "Surrounding rock pressure of shallow-buried bilateral bias tunnels under earthquake", *Geomech. Eng.*, **9**(4), 427-445.

Mazek, S.A. (2014), "Evaluation of surface displacement equation due to tunneling in cohesionless soil", *Geomech. Eng.*, **7**(1), 55-73.

Nawel, B. and Salah, M. (2015), "Numerical modeling of two parallel tunnels interaction using three-dimensional Finite Elements Method", *Geomech. Eng.*, **9**(6), 775-791.

Nikadat, N. and Marji, M.F. (2016), "Analysis of stress distribution around tunnels by hybridized FSM and DDM considering the influences of joints parameters", *Geomech. Eng.*, **11**(2), 269-288.

Öztürk, H.T., Türkeli, E. and Durmuş, A. (2016), "Optimum design of RC shallow tunnels in earthquake zones using artificial bee colony and genetic algorithms", *Comput. Concrete*, **17**(4), 435-453.

Picoux, B. (2002), "Etude théorique et expérimentale de la propagation dans le sol des vibrations émises par un trafic ferroviaire", Ph.D. Dissertation, Ecole Centrale of Nantes, Nantes, France (in French).

Picoux, B. and Le Houédec, D. (2005), "Diagnosis and prediction of vibration from railway trains", *Soil Dyn. Earthq. Eng.*, **25**(12), 905-921.

SAP2000® Version 17 (2015), *Integrated Software for Structural Analysis and Design*, Computers and Structures, Inc., Walnut Creek, California and New York, U.S.A., <https://www.csiamerica.com/products/sap2000>.

Sevim, B. (2013), "Assessment of 3D earthquake response of the Arhavi Highway tunnel considering soil-structure interaction", *Comput. Concrete*, **11**(1), 51-61.

Wells, L.G. and Treesuwan, O. (1978), "The response of various soil strength indices to changing water content and bulk density", *T. ASAE*, **21**(5), 854-861.

Yang, X.L. and Li, W.T. (2017), "Reliability analysis of shallow tunnel with surface settlement", *Geomech. Eng.*, **12**(2), 1243-1252.

Yang, X.L., Xu, J.S., Li, Y.X. and Yan, R.M. (2016), "Collapse mechanism of tunnel roof considering joined influences of nonlinearity and non-associated flow rule", *Geomech. Eng.*, **10**(1), 21-35.

Yoo, C. (2016), "Effect of spatial characteristics of a weak zone on tunnel deformation behavior", *Geomech. Eng.*, **11**(1), 41-58.

Yuan, Y.C., Li, S.C., Zhang, Q.Q., Li, L., Shi, S.S. and Zhou, Z.Q. (2016), "Risk assessment of water inrush in karst tunnels based on a modified grey evaluation model: Sample as Shangjiawan tunnel", *Geomech. Eng.*, **11**(4), 493-513.

Zhao, H., Liu, X., Bao, Y. and Yuan, Y. (2017), "Nonlinear simulation of tunnel linings with a simplified numerical modelling", *Struct. Eng. Mech.*, **61**(5), 593-603.

Zheng, G., Du, Y., Cheng, X., Diao, Y., Deng, X. and Wang, F. (2017), "Characteristics and prediction methods for tunnel deformations induced by excavations", *Geomech. Eng.*, **12**(3), 361-397.

Zhou, X., Hu, H., Jiang, B., Zhou, Y. and Zhu, Y. (2016), "Numerical analysis on stability of express railway tunnel portal", *Struct. Eng. Mech.*, **57**(1), 1-20.

CC